Journal of Solid State Chemistry 184 (2011) 2047–2052

Contents lists available at ScienceDirect

Journal of Solid State Chemistry

journal homepage: www.elsevier.com/locate/jssc

Morphology evolution of ZrB_2 nanoparticles synthesized by sol–gel method

Yun Zhang [a], Ruixing Li [a,*], Yanshan Jiang [a], Bin Zhao [a], Huiping Duan [a], Junping Li [b], Zhihai Feng [b]

[a] Key Laboratory of Aerospace Materials and Performance (Ministry of Education), School of Materials Science and Engineering, Beihang University, Beijing 100191, China
[b] Aerospace Research Institute of Materials & Processing Technology, Beijing 100076, China

ARTICLE INFO

Article history:
Received 16 February 2011
Received in revised form
7 May 2011
Accepted 29 May 2011
Available online 7 June 2011

Keywords:
Nanoparticles
Synthesis
Sol–gel
Zirconium diboride
Morphology

ABSTRACT

Zirconium diboride (ZrB_2) nanoparticles were synthesized by sol–gel method using zirconium *n*-propoxide ($Zr(OPr)_4$), boric acid (H_3BO_3), sucrose ($C_{12}H_{22}O_{11}$), and acetic acid (AcOH). Clearly, it was a non-aqueous solution system at the very beginning of the reactions. Here, AcOH was used as both chemical modifier and solvent to control $Zr(OPr)_4$ hydrolysis. Actually, AcOH could dominate the hydrolysis by self-produced water of the chemical propulsion, rather than the help of outer water. $C_{12}H_{22}O_{11}$ was selected, since it can be completely decomposed to carbon. Thus, carbon might be accounted precisely for the carbothermal reduction reaction. Furthermore, we investigated the influence of the gelation temperature on the morphology of ZrB_2 particles. Increasing the gelation temperature, the particle shapes changed from sphere-like particles at 65 °C to a particle chain at 75 °C, and then form rod-like particles at 85 °C. An in-depth HRTEM observation revealed that the nanoparticles of ZrB_2 were gradually fused together to evolve into a particle chain, finally into a rod-like shape. These crystalline nature of ZrB_2 related to the gelation temperature obeyed the "oriented attachment mechanism" of crystallography.

1. Introduction

Zirconium diboride (ZrB_2) is one of the materials known as ultra-high-temperature ceramics. It has a series of excellent properties, such as a high melting temperature (3040 °C), an outstanding wear, and a corrosion resistance. The unique combination of properties makes ZrB_2 a promising candidate for thermal protection materials, cutting tools, high temperature electrodes, and molten metal crucibles [1–5]. However, the applications of ZrB_2 ceramic material have been limited by the features of the ZrB_2 powder, such as size, purity, etc.

Traditionally, ZrB_2 powder can be synthesized mainly by the following methods: (i) solid-state reaction synthesis [6,7]; (ii) electrochemical synthesis [8]; (iii) mechanochemical synthesis [9]; and (iv) self-propagating high-temperature synthesis [10,11]. However, such processes need a higher temperature or a long production period, and furthermore the synthesized powders usually have a relatively coarse particle and a low purity. As a result, the sinterability of ZrB_2 ceramic tends to be deteriorated. Therefore, a synthesis method to reduce particle size and increase the purity of the ZrB_2 powder is needed. In contrast with those traditional methods, the sol–gel method is one of the potential methods for synthesizing ceramic materials with a fine particle size and a high purity. And it is an effective way for low temperature synthesis of ultra-fine powders. Furthermore, the advantage of using sol–gel method is that high chemical and phase homogeneity can be achieved by mixing the starting components at the molecular or colloidal level. Recently, many ultra-fine ceramic particles such as TiB_2 [12], ZrC [13], and SiC [14] were synthesized by sol–gel method. However, a little has been reported about the synthesis of ZrB_2 powder using a wet chemical process. Yan et al. [15] synthesized ZrB_2 powder using zirconium oxychloride ($ZrOCl_2 \cdot 8H_2O$), boric acid (H_3BO_3), and phenolic resin by sol–gel method. Wang et al. [16,17] synthesized ZrB_2 powder using $ZrOCl_2 \cdot 8H_2O$, boron carbide (B_4C), and carbon by wet chemical method. Additionally, Xie et al. [18] prepared ZrB_2 powder depending on the starting materials of zirconium *n*-propoxide ($Zr(OPr)_4$), H_3BO_3, and phenolic resin by sol–gel method. However, most alkoxides are known to react spontaneously with water to form a viscous precipitate; therefore, they require to be chemically modified in order to control their hydrolysis and condensation. In the case of ZrB_2, gel precursor might be obtained by hydrolysis of $Zr(OPr)_4$ chemically modified by acetylacetone (*acac*) [18]. Nevertheless, most researchers pointed out the formation of oxycarbides with relatively high oxygen content, highly detrimental for mechanical application using *acac* as a modifier. Another way to control the alkoxides hydrolysis was to use acetic acid (AcOH) as a chemical modifier. Such a sol–gel process was already investigated for TiC [19] synthesis and a low oxygen content of TiC was reported.

* Corresponding author. Fax: + 86 10 8231 6500.
E-mail address: ruixingli@yahoo.com (R. Li).

0022-4596/$ - see front matter © 2011 Elsevier Inc. All rights reserved.
doi:10.1016/j.jssc.2011.05.040

However, little has been reported on AcOH as a modifier for the ZrB_2 synthesis.

This paper deals with the discussion of a new sol–gel method, using AcOH as both a modifier and a unique solvent to control $Zr(OPr)_4$ hydrolysis to synthesize ZrB_2 particles. $Zr(OPr)_4$ and H_3BO_3 were the sources of zirconium (Zr) and boron (B), respectively. Sucrose ($C_{12}H_{22}O_{11}$) was a source of pyrolyzed carbon. Here, $C_{12}H_{22}O_{11}$ was used, since it can be completely decomposed to carbon. Thus, carbon might be accounted precisely, as a consequence, the molar ratio of C/Zr might be fixed. In contrast, the char yield of phenolic resin, which is used as another source of pyrolyzed carbon is not fixed (about 50 wt%). It is notable that no aqueous solvent or hydrated compound was accommodated into the starting materials. In other words, it was a non-aqueous solution system at the very beginning of the reactions. Furthermore, the mechanism of stabilizing $Zr(OPr)_4$ by AcOH and the influence of the gelation temperature on the morphology of ZrB_2 particles were investigated.

2. Experimental

2.1. Starting materials

$Zr(OPr)_4$ with a concentration of 70 wt% was supplied by the Shanghai Jingchun Reagents Co. Ltd., Shanghai, China. H_3BO_3, $C_{12}H_{22}O_{11}$, and AcOH were supplied by the Lanyi Reagents Co. Ltd., Beijing, China. The grade of all the above reagents was analytical.

2.2. Synthesis

A general flow diagram for the synthesis of ZrB_2 powder is shown in Fig. 1. In a typical synthesis, 2.4 g of H_3BO_3 and 2.5 g of $C_{12}H_{22}O_{11}$ were dissolved in 35 ml of AcOH using a 80 ml beaker. Then, it was heated with vigorous stirring to 80 °C and maintained for 0.5 h. We refer to this solution as Mixed solution 1. Afterwards, 5.7 g of $Zr(OPr)_4$ were added to the Mixed solution 1, which was previously cooled to room temperature. This was Mixed solution 2. The Mixed solution 2 was heated with vigorous stirring to 65 °C (This fixed temperature is so-called gelation temperature to form sol/gel. 75 and 85 °C were also set in the final section of this paper.) and maintained for 3 h to form a wet gel. Finally, it was dried under vacuum at 120 °C for 3 h followed by a grind process using an agate mortar and a pestle. In this way, a precursor powder was prepared.

After that, the above precursor was firstly heated to 800 °C at a heating rate of 5 °C/min, then to 1200 °C at 3 °C/min and maintained at this temperature for 2 h in argon using an alumina tube furnace. Afterwards, the precursor powder was continued to heat from 1200 to 1550 °C at a heating rate of 2 °C/min and kept at this temperature for 2 h. Then, the sample was cooled to room temperature at a cooling rate of 5 °C/min. In the end, gray powder was obtained.

2.3. Characterization

The mass and heat flow of the samples were monitored by thermal analysis (TG-DTA, Beijing Hengjiu instrument Co. Ltd., Beijing, China). The crystallographic constitution was identified by means of an X-ray diffractometer (XRD) using graphite monochromatized Cu$K\alpha$ radiation (Rigaku, D/MAX 2200 PC). Chemical analysis was performed using infrared method (America, PC600). Crystallite size was estimated using the Debye–Scherrer equation,

$$D_{hkl} = 0.9\lambda/\beta_{hkl}\cos\theta \quad (1)$$

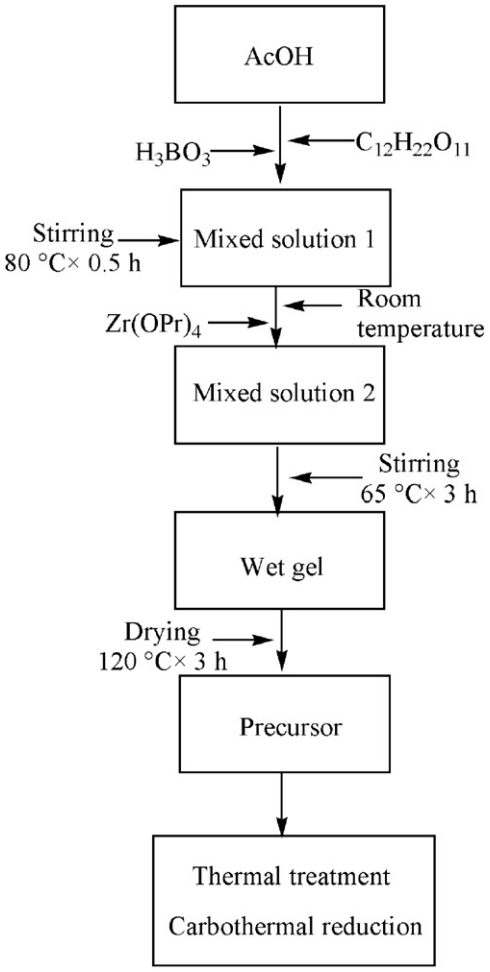

Fig. 1. General flow diagram for synthesis of ZrB_2 powder.

where D_{hkl} is the crystallite size, λ is the wavelength of Cu$K\alpha$ radiation, β_{hkl} is the full-width at half maximum, and θ is the Bragg diffraction angle. The morphology of the final products was characterized by SEM using a JEOL JSM-6700F JAPAN microscope and TEM using a JEM-2100F microscope.

3. Results and discussion

3.1. AcOH dependent mechanism

Theoretically, inorganic metal salts or metal organic compounds such as metal alkoxides are combined with a mixture of solvents to form a sol or a gel in sol–gel processes. As a consequence, the metal organic compounds are partially or completely hydrolyzed and condensed. However, metal alkoxides are well known to react spontaneously with water and to form precipitates resulting from successive hydrolysis. In order to obtain a sol/gel, $Zr(OPr)_4$ has to be chemically modified by a complexing agent to decrease the alkoxide reactivity with water. Several works [13,19–22] had shown that metal alkoxides could be modified by AcOH as bridging and chelating ligands to forming acetates by the substitution of *OAc* for *OPr* groups. Additionally, AcOH was also used for controlling the sol–gel processes by self-produced water without the help of outer water [23,24]. That is to say, the water for hydrolysis was generated in situ by esterification of AcOH with alcohol released by the preceding formation of acetate derivatives of the alkoxides.

To explore the action of AcOH on the other reactants, the general reactions occurring during the precursor preparation are metal chelate formation, transesterification, and hydrolysis-condensation. The first reaction was the formation of zirconium propoxide diacetate $Zr(OAc)_2(OPr)_2$ (see Eq. (2)) [25]:

(2)

This carboxylatoalkoxide could then react following different competitive reactions. The first one was the transesterification of alkoxy groups in $Zr(OAc)_2(OPr)_2$, which reacted with the sucrose *OH* groups according to Eq. (3):

(3)

where *X* is a simplified notation for $C_{12}H_{14}O_3$.

The second reaction occurred between the unreacted AcOH and the propanol, which was one of the products of the reactions (2) and (3) to form water and propyl acetate (see Eq. (4)):

$$AcOH + PrOH \rightarrow PrOAc + H_2O \quad (4)$$

The water and the zirconium propoxide diacetate, which was one of the products of the reaction (2) reacted spontaneously in a substitution reaction (see Eq. (5)), in which hydroxy groups replaced propoxy groups to generate propanol.

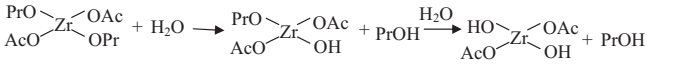

(5)

As the water produced in reaction (4) was consumed for the hydrolysis, the equilibrium of Eq. (4) was then driven to the right as long as sufficient AcOH was present in the solution. Another reaction, which might occur, was the generation of oxo ligands by non-hydrolytic condensation and elimination of an ester. Once the different molecules with hydroxy groups formed $Zr(OPr)_2(OH)_2$, and $Zr(OAc)_2(OPr)$–O–X–$(OH)_7$, further condensation reactions occurred leading to an increase of the solution viscosity associated to the formation of Zr–O–Zr and Zr–O–X–O–Zr bridges. A polymeric precursor was obtained and was placed under heating at 65 °C for 3 h to evaporate the residual AcOH and the acetates products. After both drying and grinding steps, a precursor powder was obtained.

3.2. Thermal analysis of precursor powder

First of all, TG-DTA analysis of precursor powder in argon was conducted to understand the processes of pyrolysis of the precursor. The complementary information obtained allows differentiation between endothermic and exothermic events, which have no associated weight loss (e.g. melting and crystallization) and those which involve a weight loss (e.g. degradation). TG analysis showed that a considerable weight loss occurred in a temperature range of 100–550 °C for the precursor, as shown in Fig. 2. An in-depth analysis showed that the weight loss was *ca.* 8.0% from 100 to 240 °C, and *ca.* 25% from 240 to 550 °C (see Fig. 2). To clarify why the weight loss occurred during heating, the reaction (6) has to be considered firstly, although it had finished during the process in which the wet gel was dried under vacuum at 120 °C.

$$H_3BO_3(s) \rightarrow HBO_2\ (s) + H_2O\ (g)\uparrow \quad (6)$$

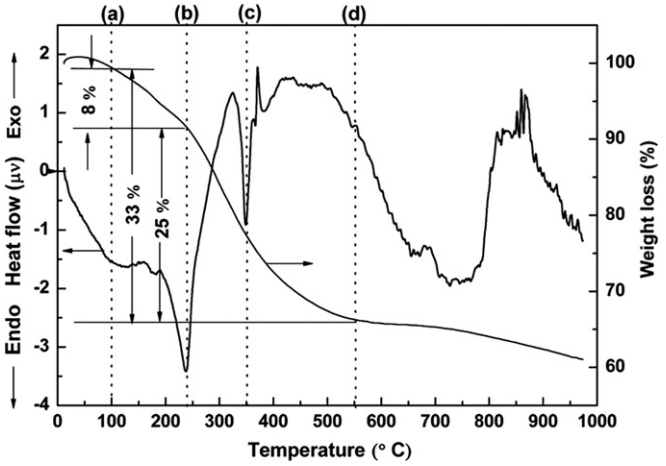

Fig. 2. TG-DTA thermal analysis curve for ZrB_2 precursor from room temperature to 1000 °C. (a) 100 °C; (b) 240 °C; (c) 350 °C; (d) 550 °C. (Gelation temperatures: 65 °C, B/Zr (mol)=2.3).

Taking all results into account, the thermal decomposition reactions between 100 and 550 °C may be described as follows:

$$2HBO_2\ (s) \rightarrow B_2O_3\ (l) + H_2O\ (g)\uparrow \quad (7)$$

$$C_{12}H_{22}O_{11}\ (s) \rightarrow 12C\ (s) + 11H_2O\ (g)\uparrow \quad (8)$$

In the present reaction system, HBO_2 completely decomposed to B_2O_3 and H_2O, accompanied with 6.1% weight loss between 100 and 240 °C (see Eq. (7)). $C_{12}H_{22}O_{11}$ completely transformed to carbon and H_2O, accompanied with 23.6% weight loss between 240 and 550 °C (see Eq. (8)). Totally, the theoretical weight loss was 29.7% in the temperature range of 100–550 °C. This magnitude is almost in agreement with the experimental weight loss of 33% between 100 and 550 °C (see Fig. 2).

Alternatively, DTA curve in Fig. 2 reveals that an endothermic peak at about 240 °C. It might be attributed to both the evaporation of the bonded water and the decomposition of HBO_2. Another endothermic peak at about 350 °C was due to the complete carbonization of $C_{12}H_{22}O_{11}$. The inflection in a temperature range of 650–780 °C was due to crystallization of amorphous ZrO_2 to tetragonal ZrO_2 [26]. With the increasing of the temperature, several exothermic peaks in a temperature ramp from 820 to 880 °C could be attributed to the delayed crystallization of ZrO_2 [27].

3.3. Influence of pyrolysis/calcination temperature on phase constitution

The phase constitution before and after pyrolysis/calcination was identified based on the above results of the thermal analysis. Fig. 3 shows XRD patterns of the precursor powder calcined at different temperatures. Clearly, the precursor was in a typical amorphous state without any peak in its XRD pattern (see Fig. 3(a)). In contrast, increasing the pyrolysing/calcining temperature, the powder gradually crystallized. In the sample treated at 1100 °C for 2 h, *m*-ZrO_2 and *t*-ZrO_2 phases were identified (see Fig. 3(b)). Both XRD and TG-DTA results showed that the precursor was probably transformed to ZrO_2, B_2O_3, and carbon at 1100 °C [28]. However, there was no trace of B_2O_3 and carbon phases in the diffraction patterns. That is to say, the temperature was not high enough to initiate a completely carbothermal reduction, and both B_2O_3 and carbon phases might be amorphous. ZrB_2 was generated at 1300 °C as shown in Fig. 3(c). With the increasing of the calcining temperature, the XRD patterns showed that the diffraction intensity of ZrB_2 increased, *m*-ZrO_2 and *t*-ZrO_2

decreased. Finally, a single phase of ZrB_2 was evolved at 1550 °C for 2 h (see Fig. 3(e)). This means that a carbothermal reduction process was able to complete at 1550 °C. A further study was conducted to evaluate the average particle/grain size based on the Debye–Scherrer equation. The result revealed that was about 62 nm.

Theoretically, an idealized reaction to produce ZrB_2 by carbothermal reduction in the present study is shown as follows:

$$ZrO_2\,(s)+B_2O_3\,(g)+5C\,(s)\rightarrow ZrB_2\,(s)+5CO\,(g)\uparrow \quad (9)$$

Here, B_2O_3 has an unusual low melting point (450 °C) and a high vapor pressure. The vapor pressure of B_2O_3 at 1527 °C reaches 344 Pa, leading to its rapid vaporization [29]. Therefore, a higher B/Zr ratio for the starting materials that the stoichiometric proportion of B/Zr (mol)=2.0 as shown in reaction (9) is necessary. On the basis of our investigation, the optimum ratio of B/Zr was experimentally determined as 2.3, and this value was used in this study (full text).

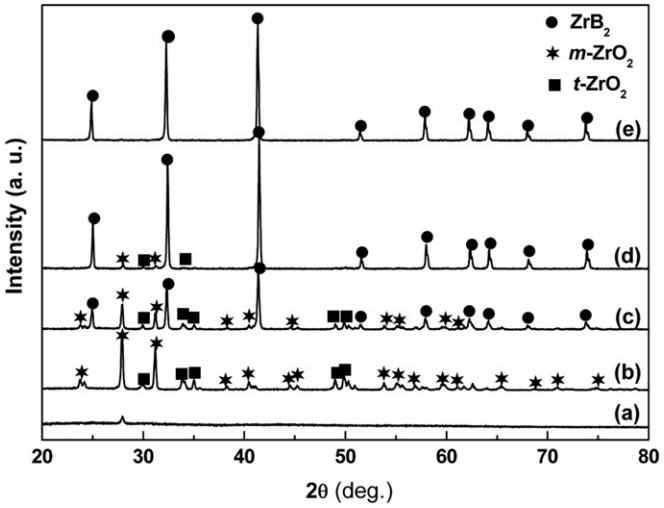

Fig. 3. XRD patterns of (a) precursor, and the precursor reduced carbothermally at (b) 1100 °C; (c) 1300 °C; (d) 1400 °C; (e) 1550 °C. (Gelation temperatures: 65 °C, B/Zr (mol)=2.3).

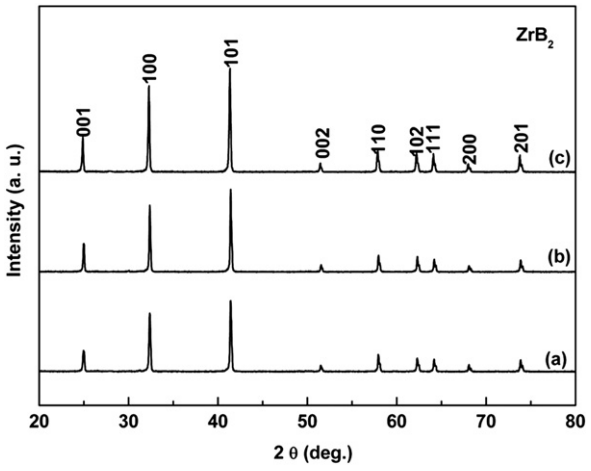

Fig. 4. XRD patterns of the precursor powder reduced carbothermally at 1550 °C for 2 h with gelation temperatures of (a) 65 °C; (b) 75 °C; (c) 85 °C. (B/Zr (mol)=2.3).

3.4. Influence of gelation temperature on morphology of ZrB_2

It is well known that the gelation temperature is an important factor for both nucleation and crystal feature. Here, different gelation temperatures of 65, 75, and 85 °C were fixed to synthesize ZrB_2 powder. Fig. 4 shows XRD patterns of the powder

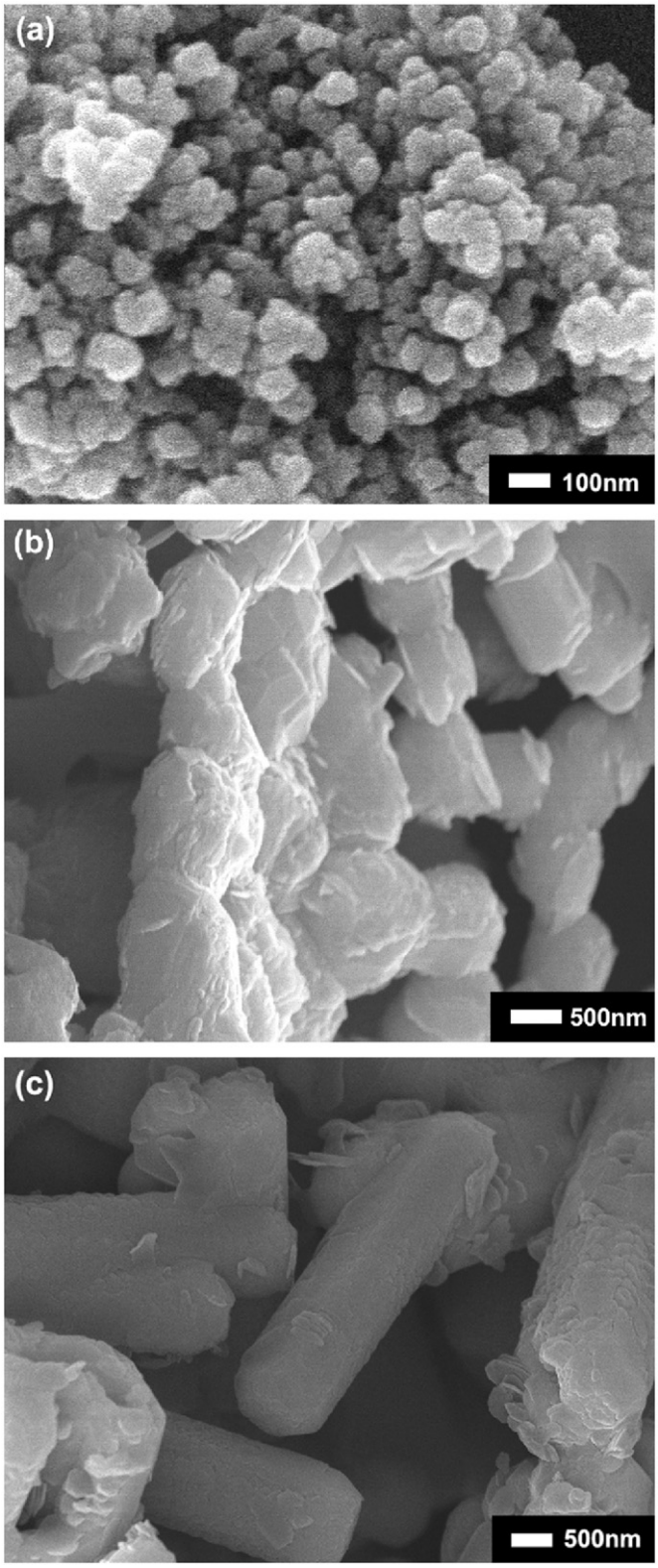

Fig. 5. SEM images of ZrB_2 powder reduced carbothermally at 1550 °C for 2 h with gelation temperatures of (a) 65 °C; (b) 75 °C; (c) 85 °C. (B/Zr (mol)=2.3).

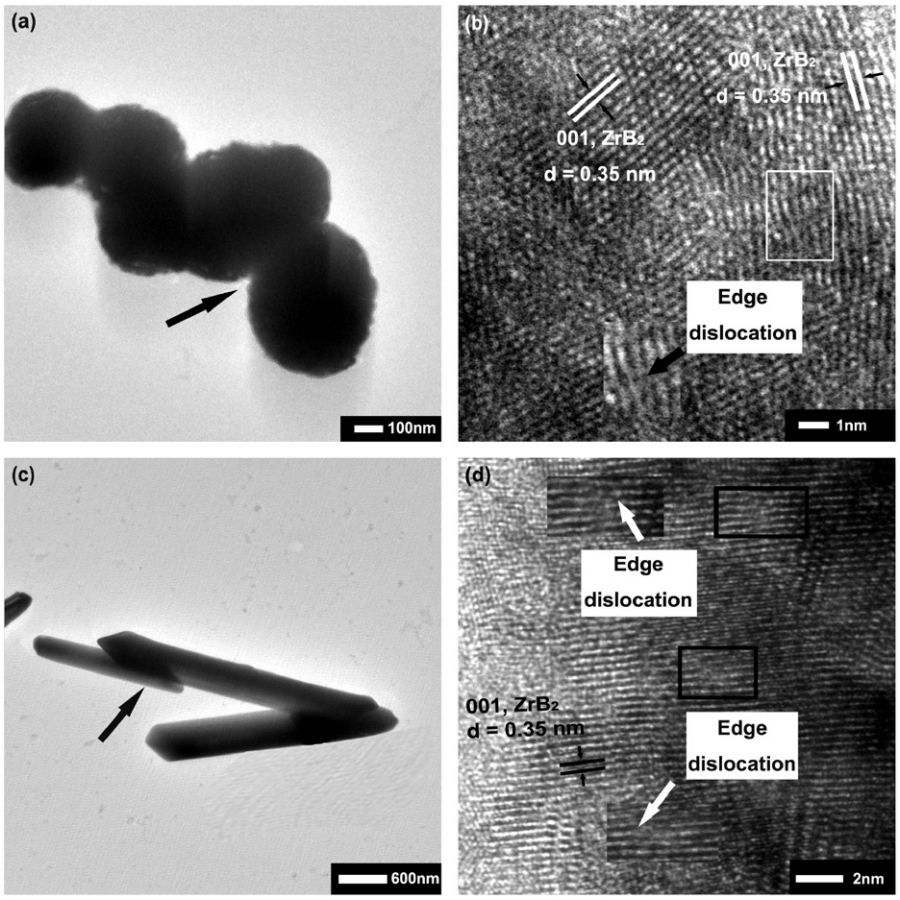

Fig. 6. TEM images of ZrB_2 powder reduced carbothermally at 1550 °C for 2 h with gelation temperatures of (a) 75 °C; (c) 85 °C; (b) HRTEM image of ZrB_2 particle chain marked in (a); (d) HRTEM images of rod-like ZrB_2 marked in (c). (B/Zr (mol)=2.3).

precursor calcined at 1550 °C for 2 h with different gelation temperature and a molar ratio of B/Zr=2.3. It might be seen that all of the diffraction peaks were well assigned to a single phase of ZrB_2.

Furthermore, the influence of the gelation temperature on the morphology of the samples was also investigated, and the SEM images of the as-calcined samples are shown in Fig. 5. It is observed that the morphology of the samples was affected by the gelation temperature. For the ZrB_2 sample gelated at 65 °C, the SEM revealed a sphere-like morphology of ZrB_2 nanoparticles (see Fig. 5(a)). At 75 °C, the morphology showed a particle chain (see Figs. 5(b) and 6(a)). With the increasing of the temperature to 85 °C, the morphology of the ZrB_2 particles evolved to a rod-like shape. Additionally, the size of ZrB_2 particle also increased notably with the increasing of the gelation temperature.

To explain the morphology influenced by the gelation temperature requires a multidisciplinary knowledge. A further investigation, a high-resolution TEM (HRTEM), was conducted to clarify the microstructure and crystal feature of the ZrB_2 particles. At a lower temperature, the rate of nucleation was faster than that of growth, whereas the monomer concentration was sharply decreased [30]. Such slow growth conditions favored the formation of a sphere-like shape (see Fig. 5(a)). With increasing the gelation temperature, Figs. 5(b) and 6(a) show that a particle chain of ZrB_2 was evolved at 75 °C. The HRTEM image of ZrB_2 particle chain revealed that each unique particle chain was composed of several sphere-like particles. These sphere-like particles aligned one by one to form a polycrystalline particle chain of ZrB_2 and shared a quasi-parallel crystal orientation at the grain interfaces (see Fig. 6(a) and (b)). It is notable that the interface between the two grains in the rectangle region (magnified in Fig. 6(b)) involved edge dislocations (arrowhead). With the temperature further increased, adjacent particles fused together to form strong links resulting in the evolution of ZrB_2 rods (see Figs. 5(c) and 6(c)). In the same way, the adjacent grains shared a common crystallographic orientation, followed by joining of these grains at a planar interface with edge dislocations (arrowhead) (see Fig. 6(d)). It also may be found from the HRTEM image that these particle chain/rod shared {0 0 1} lattice fringes with interplanar spacings of 0.35 nm.

From a crystallography perspective, according to the "oriented attachment mechanism", which was first explored by Penn and Banfield [31], adjacent particles share a common crystallographic orientation, followed by joining of these particles at a planar interface. Bonding between adjacent nanoparticles reduces the overall energy by removing the surface energy associated with unsatisfied bonds. Clearly, this attachment mechanism is reflected by the results in Fig. 6. The ZrB_2 nanoparticles connected with each other via the "oriented attachment mechanism" and a reduction in surface free energy was achieved by the complete removal of pairs of surfaces. Imperfect oriented attachment of nanocrystals can generate dislocations. Any defects observed by HRTEM can be attributed to the growth process.

4. Conclusions

ZrB_2 nanoparticles were synthesized by sol–gel method using AcOH as both chemical modifier and solvent to control $Zr(OPr)_4$ hydrolysis in the absence of water for the starting materials. It is notable that a single phase ZrB_2 could be obtained with a molar ratio of B/Zr=2.3 for the starting materials at 1550 °C for 2 h.

Sphere-like, particle chain, and rod-like ZrB_2 particles could be obtained synthesized at different gelation temperatures: 65, 75, and 85 °C. In an effort to understand the mechanism of morphology evolution, the "oriented attachment mechanism" might explain the crystalline processes of ZrB_2 particles based on the HRTEM observation.

Acknowledgments

The authors appreciate the financial support from the National Science Foundation of China (NSFC50974007); the Scientific Research Starting Foundation for Returned Overseas Chinese Scholars, Ministry of Education; the Start-Up Fund for High-End Returned Overseas Talents, Ministry of Human Resources and Social Security, China (Renshetinghan 2010, No. 411); and the Lab-Installation Foundation of Beihang University for New Teachers (No. 280101).

References

[1] F. Monteverde, S. Guicciardi, A. Bellosi, Mater. Sci. Eng. A. 346 (2003) 310–319.
[2] S.R. Levine, E.J. Opila, M.C. Halbig, J.D. Kiser, M. Singh, J.A. Salem, J. Eur. Ceram. Soc. 22 (2002) 2757–2767.
[3] M.M. Opeka, I.G. Talmy, J.A. Zaykoski, J. Mater. Sci. 39 (2004) 5887–5904.
[4] S. Norasetthekul, P.T. Eubank, W.L. Bradley, B. Bozkurt, B. Stucker, J. Mater. Sci. 34 (1999) 1261–1270.
[5] C. Mroz, Am. Ceram. Bull. 76 (1995) 164–165.
[6] Z.A. Munir, Am. Ceram. Soc. Bull. 67 (1988) 342–349.
[7] S.K. Mishra, S. Das, P. Ramchandrarao, J. Mater. Res. 17 (2002) 2809–2814.
[8] H. Zhao, Y. He, Z.Z. Jin, J. Am. Ceram. Soc. 78 (1995) 2534–2536.
[9] N. Setoudeh, N.J. Welham, J. Alloys Comp. 420 (2006) 225–228.
[10] H.E. Camurlu, F. Maglia, J. Eur. Ceram. Soc. 29 (2009) 1501–1506.
[11] T. Tsuchida, S. Yamamoto, J. Eur. Ceram. Soc. 24 (2004) 45–51.
[12] L'. Băca, N. Stelzer, J. Eur. Ceram. Soc. 28 (2008) 907–911.
[13] M. Dollĕe, D. Gosset, C. Bogicevic, F. Karolak, D. Simeone, G. Baldinozzi, J. Eur. Ceram. Soc. 27 (2007) 2061–2067.
[14] G.W. Meng, L.D. Zhang, C.M. Mo, S.Y. Zhang, H.J. Li, Y. Qin, S.P. Feng, Metall. Trans. A 30A (1999) 213–219.
[15] Y.J. Yan, Z.R. Huang, S.M. Dong, D.L. Jiang, J. Am. Ceram. Soc. 89 (2006) 3585–3588.
[16] C.A. Wang, H.L. Wang, L. Yu, Y. Huang, Mater. Sci. Forum (561 – 565) (2007) 523–526.
[17] H.L. Wang, S.X. Zhang, D.L. Chen, Q.F. Han, H.X. Lu, C.A. Wang, R. Zhang, Adv. Mater. Res. 105 – 106 (2010) 203–206.
[18] Y.L. Xie, H. Thomas Jr., S. Sanders, F. Robert, J. Am. Ceram. Soc. 91 (2008) 1469–1474.
[19] H. Preiss, L.M. Berger, D. Schultze, J. Eur. Ceram. Soc. 19 (1999) 195–206.
[20] S. Doeuff, M. Henry, C. Sanchez, J. Livage, J. Non-Cryst. Solids 89 (1987) 206–216.
[21] J. Livage, M. Henry, C. Sanchez, Prog. Solid State Chem. 18 (1988) 259–341.
[22] C. Sanchez, J. Livage, M. Henry, F. Baboneau, J. Non-Cryst. Solids 100 (1988) 65–76.
[23] H. Schmidt, B. Seiferling, Mater. Res. Soc. Symp. Proc. 73 (1986) 739–750.
[24] S. Doeu, Y. Dromzee, F. Taulelle, C. Sanchez, Inorg. Chem. 28 (1989) 4439–4445.
[25] G. Yi, M. Sayer, J. Sol–Gel Sci. Technol. 6 (1996) 65–74.
[26] H. Preiss, L.M. Berger, K. Szulzewsky, Carbon 34 (1996) 109–119.
[27] H. Preiss, D. Schultze, P. Klobes, J. Eur. Ceram. Soc. 17 (1997) 1423–1435.
[28] S.M. Yun, K. Palanivelu, Y.H. Kim, K.H. Kang, Y.S. Lee, J. Ind. Eng. Chem. 14 (2008) 667–671.
[29] W.G. Fahrenholtz, J. Am. Ceram. Soc. 88 (2005) 3509–3512.
[30] L. Manna, E.C. Scher, A.P. Alivisatos, J. Am. Chem. Soc. 122 (2000) 12700–12706.
[31] R.L. Penn, J.F. Banfield, Science 281 (1998) 969–971.